Monthly Notices of the ROYAL ASTRONOMICAL SOCIETY
MNRAS **455,** 1334–1340 (2016) doi:10.1093/mnras/stv2362

TraMoS – IV. Discarding the Quick Orbital Decay Hypothesis for OGLE-TR-113b

S. Hoyer,[1,2⋆] M. López-Morales,[3⋆] P. Rojo,[4⋆] D. Minniti[5,6,7,8] and E. R. Adams[9]

[1]*Instituto de Astrofísica de Canarias, E-38205 La Laguna, Tenerife, Spain*
[2]*Dpto. Astrofísica, Universidad de La Laguna, E-38206 La Laguna, Tenerife, Spain*
[3]*Harvard–Smithsonian Center for Astrophysics, 60 Garden Street, Cambridge, MA 01238, USA*
[4]*Departamento de Astronomía, Universidad de Chile, Casilla 36-D, Santiago, Chile*
[5]*Departamento de Ciencias Físicas, Universidad Andrés Bello, República 220, Santiago, Chile*
[6]*Vatican Observatory, I-V00120 Vatican City State, Italy*
[7]*Millennium Institute for Astrophysics, Santiago, RM, Chile*
[8]*Pontificia Universidad Católica de Chile, Instituto de Astrofísica, Av. Vicuña Mackenna 4860, Santiago, Chile*
[9]*Planetary Science Institute, 1700 East Fort Lowell, Suite 106, Tucson, AZ 85719, USA*

Accepted 2015 October 8. Received 2015 October 5; in original form 2014 November 5

ABSTRACT

In the context of the Transit Monitoring in the South project, we present nine new transit observations of the exoplanet OGLE-TR-113b observed with the Gemini South, Magellan Baade, Danish-1.54 m and Southern Astrophysical Research telescopes. We perform a homogeneous analysis of these new transits together with 10 literature transits to probe into the potential detection of an orbital decay previously reported for this planet. Our new observations extend the transit monitoring baseline for this system by 6 yr, to a total of more than 13 yr. With our timing analysis we obtained a $\dot{P} = -1.0 \pm 6.0$ ms yr^{-1}, which rejects previous hints of a larger orbital decay for OGLE-TR-113b. With our updated value of $\dot{P}$ we can discard tidal quality factors of $Q_\star < 10^5$ for its host star. Additionally, we calculate a 1σ dispersion of the transit timing variations of 42 s over the 13 yr baseline, which discards additional planets in the system more massive than 0.5–3.0 $M_\oplus$ in 1:2, 5:3, 2:1 and 3:1 Mean Motion Resonances with OGLE-TR-113b. Finally, with the joint analysis of the 19 light curves we update transit parameters, such as the relative semimajor axis $a/R_s = 6.44^{+0.04}_{-0.05}$, the planet-to-star radius ratio $R_p/R_s = 0.14436^{+0.00096}_{-0.00088}$, and constrains its orbital inclination to $i = 89.27^{+0.51}_{-0.68}$ deg.

Key words: methods: data analysis – techniques: photometric – ephemerides – time – planets and satellites: individual: OGLE-TR-113b.

1 INTRODUCTION

OGLE-TR-113b was one of the first discovered transiting exoplanets, reported by Udalski et al. (2002) as a planet candidate orbiting a $V = 16.1$ K-dwarf star, and later confirmed by Bouchy et al. (2004) and Konacki et al. (2004) via radial velocity follow-up campaigns. With a mass of 1.23 $M_{\rm Jup}$ and a radius of 1.09 $R_{\rm Jup}$ (Southworth 2012), OGLE-TR-113b is a hot Jupiter orbiting its host star once every 1.43 d. Due to the proximity to its host star, OGLE-TR-113b is potentially an interesting target for orbital decay by tidal dissipation studies (see e.g. Sasselov 2003; Pätzold, Carone & Rauer 2004; Carone & Pätzold 2007; Levrard, Winisdoerffer & Chabrier 2009; Matsumura, Peale & Rasio 2010; Penev & Sasselov 2011; Penev et al. 2012), in which it is predicted that the orbital separation between the star and the planet will continue to shrink – in spite of orbital circularization – as long as the orbital motion of the planet is faster than the stellar rotation rate. In those cases, the planet's orbital decay will continue until the planet reaches the stellar Roche radius limit of the system and falls into the star (see e.g. Levrard et al. 2009).

Although the orbital decay of exoplanets is a topic that has received increasing attention over the past decade, estimations of the expected time-scales of this effect remain largely unconstrained because of the currently limited understanding and measurements of tidal dissipation mechanisms in both planets and stars. Because of this lack of understanding, tidal quality factors, which are a measure of the star or planet's distortion due to tidal effects and drive the efficiency of the orbital time decay, are generally allowed to adopt a wide range of values, between $Q_\star = 10^4$–10^{10} (see e.g. Pätzold et al. 2004; Matsumura et al. 2010).

Directly measuring the orbital decay of a close-in, short period, exoplanet would enable the first empirical test to current tidal stability and dynamical models of these objects. A way to detect that orbital decay is via long-term monitoring campaigns of transiting

⋆E-mail: shoyer@iac.es (SH); mlopez-morales@cfa.harvard.edu (ML-M); projo@das.uchile.cl (PR)

Table 1. Description of each of the nine new transit observations presented in this work.

Epoch	Date Obs. (yyyymmdd)	Instrument / Telescope	Filter	Average cadence (s)	Airmass range	# points
192	20060104	GMOS/Gemini-S	*g*'	75/330	2.34 – 1.18	120
946	20081219	GMOS/Gemini-S	*g*'	54	2.07 – 1.29	180
953	20081229	GMOS/Gemini-S	*g*'	54	1.67 – 1.21	206
969	20090121	GMOS/Gemini-S	*g*'	54	1.65 – 1.20	213
990	20090220	GMOS/Gemini-S	*i*'	44	1.19 – 1.31	284
992	20090223	GMOS/Gemini-S	*i*'	49	1.58 – 1.17	381
1471	20110110	MagIC-e2V/Magellan	*i*'	62	1.47 – 1.19	241
2530	20150306	DFOSC/Danish-1.54 m	*R*	144	1.19 – 1.99	161
2585	20150624	SOI/SOAR	*I*	57	1.18 – 1.92	239

exoplanets in search for small and steady transit timing variations (TTVs; see e.g. Miralda-Escudé 2002; Agol et al. 2005; Holman & Murray 2005), which would show the transits occurring systematically closer in time over time-scales of several years.

Adams et al. (2010), hereafter A10, reported the tentative detection of an orbital period decay of $\dot{P} = -60 \pm 15$ ms yr^{-1} for OGLE-TR-113b, but the authors acknowledged that more observations were needed to confirm their claim. That period decay rate could be reproduced by a relatively small tidal quality factor for the star of $Q_\star \sim 10^3$–10^4 (Birkby et al. 2014), which is close to the theoretical lowest estimate for this parameter. Additionally, Penev et al. (2012) concluded that the population of currently known planets is inconsistent at the 99 per cent level with $Q_\star > 10^7$.

OGLE-TR-113b is one of the targets we have been monitoring in our Transit Monitoring in the South (TraMoS) project, which includes observations from the 1-m telescope at CTIO, Southern Astrophysical Research (SOAR) and Gemini South telescopes at Cerro Pachón Observatory (Hoyer, Rojo & López-Morales 2012). TraMoS, which has been underway since 2008, is dedicated to searching for TTVs of known planets to unveil additional planets in those systems and, therefore, their architecture. Other planetary systems we have published as part of TraMoS are OGLE-TR-111b WASP-5b and WASP-4b (see Hoyer et al. 2011, 2012, 2013).

In this work, we present eight new transit light curves of OGLE-TR-113b from TraMoS, observed with Gemini South, SOAR and Danish-1.54 m telescopes, and a new transit light curve obtained with the same instrumental setup used by A10 on Magellan. We combine those new light curves with all available literature light curves to perform a new study of TTVs for this system. In Section 2, we describe the observations. Section 3 describes the data analysis and light-curve fitting. Sections 4 and 5 describe the timing analysis and mass limits for unseen perturbers, and we present our conclusions in Section 6.

2 OBSERVATIONS AND PHOTOMETRY

We observed OGLE-TR-113b during nine transit epochs between 2006 and 2015. The first six transits were observed with the Gemini Multi-Object Spectrograph (GMOS-S) instrument on the 8.1 m Gemini South Telescope (programs ID: GS-2005B-Q-9, GS-2008B-Q-11, GS-2009A-Q-16 and GS-2010A-Q-36). GMOS-S in imaging mode has a pixel scale of 0.073 arcsec pixel^{-1} and a Field of View (FoV) of 330 × 300 arcsec^2. However, for these observations we used a Region of Interest (RoI) which includes only the central 1024 rows, reducing the readout time of the detector to only ∼47 s. The FoV of the RoI is 75 × 168 arcsec^2, which given the relatively crowded field of OGLE-TR-113b, contains enough comparison stars to perform precise differential photometry. In addition, the high resolution of the pixels minimizes blends.

The transit on 2006-01-04 ($E = 192$, where we use as $E = 0$ the transit of 2005-04-04 from Gillon et al. 2006 described below), was observed alternating between the GMOS *g*'(G0325) and GMOS *i*' (G0327) filters with exposures of 30 s each. Unfortunately, the GMOS *i*' images were saturated and are not included in this work. The next three transits were observed in the GMOS *g*'(G0325) filter and the last two epochs were observed with the GMOS *i*' (G0327) filter. Each observation lasted between 3.1 and 5.4 h, and included the full transit and out of eclipse baseline. The dates and other specific details of each transit observation are summarized in Table 1.

The transit of 2011-01-10 was observed with the MagIC-e2v camera on the 6.5 m Baade Telescope at Las Campanas Observatory, and with the same setup described in A10. MagIC-e2v has a FoV of 38 × 38 arcsec^2, with a resolution of 0.037 arcsec pixel^{-1}. The frame transfer mode of MagIC-e2v provides a readout of 0.003 s per frame, which highly surpasses the readout of conventional cameras, such as GMOS-S. The observations were done in unbinned mode, with a Sloan *i*' filter, and an exposure time of 30 s per frame. The observations lasted 4.1 h, and include the full transit and out of transit baseline.

The 2015-03-06 transit was observed using the DFOSC (Danish Faint Object Spectrograph and Camera) camera on the 1.54 m Danish Telescope at ESO La Silla Observatory. DFOSC has a FoV of 13.7 arcmin × 13.7 arcmin at a plate scale of 0.396 arcsec pixel^{-1}. We used unbinned mode, with the *Bessel R* filter and an exposure time of 100 s.

The last transit, 2015-06-24, was obtained with SOI (SOAR Optical Imager) on the 4.1 m SOAR Telescope at Cerro Pachón Observatory. SOI is a mini-mosaic of two E2V 2k × 4k CCDs with a FoV of 5.26 arcmin × 5.26 arcmin and a pixel scale of 0.077 arcsec pixel^{-1}. We used a *Bessel I* filter and an exposure time of 45 s per frame in the 2×2 binned mode. At the end of the night the sky was covered by clouds which prevented observations of the egress and after-the-transit baseline.

To reduce the data, in the case of GMOS-S we used the processed images delivered by the Gemini telescope reduction pipeline. In the case of the MagIC-e2v, DFOSC and SOI data, we bias-corrected and flatfielded the images using standard IRAF routines.

The reduced images were ran through a custom, python-based pipeline developed for TraMoS. This pipeline performs aperture photometry of the target and a set of reference stars and combines them to create differential light curves, free of most Earth atmospheric effects. The aperture radius, sky annulus and reference stars are determined iteratively by the pipeline, as those that produce

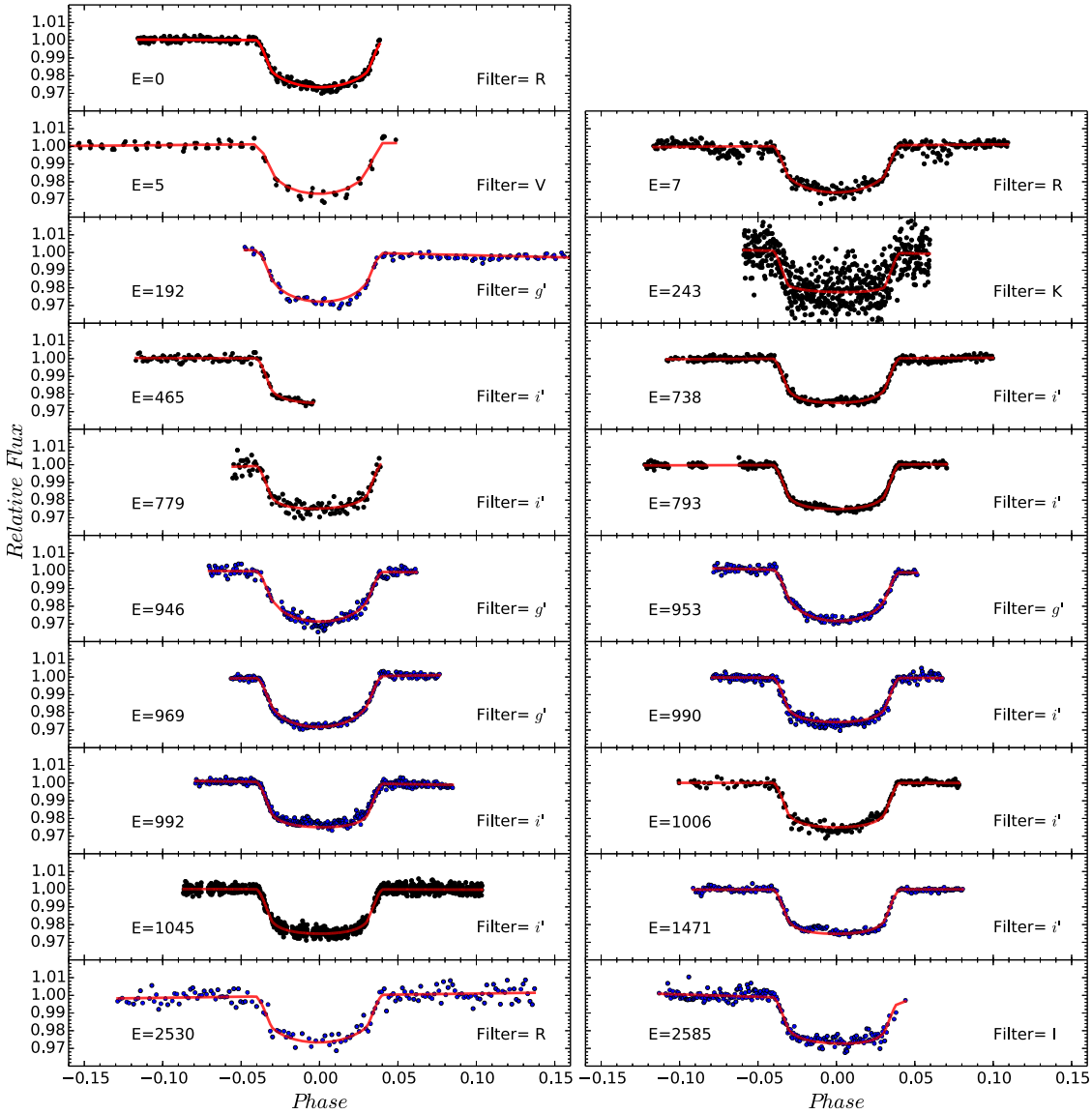

Figure 1. Transit light curves of OGLE-TR-113b. The nine transits presented in this work (blue points) are shown with the 10 literature light curves (black points). Each transit is labelled with its respective epoch and filter. The transit models obtained with TAP are shown with the red solid lines.

the smallest dispersion of the out-of-transit light curves. In some data sets, where the seeing variations during the night are large, the pipeline allows for different values of the aperture and sky annulus throughout the night. The light curves of each of the nine new transits, which still contain some systematics effects that need to be modelled (see Section 3), are shown in Fig. 1 along with the literature light curves described below.

2.1 Literature light curves

In our analysis, we also included 10 literature light curves: two light curves in *R* band collected on April 4 and 14 2005 UT (Gillon et al. 2006), a *V*-band light curve collected on 2005 April 11 UT (Diaz et al. 2007; Pietrukowicz et al. 2010), a light curve in *K* band observed on 2006 March 18 UT (Snellen & Covino 2007), and six light curves observed between 2007 January 30 UT and 2009 May 10 UT reported by A10. We used the compilation of all these light curves by A10.

3 LIGHT-CURVE MODELLING

We modelled our nine new transit light curves simultaneously with the literature light curves using the Transit Analysis Package (TAP v2.104; Gazak et al. 2012) Like in A10, we did not fit the Konacki et al. (2004) light curve, since it is the result of phase folded data from the Optical Gravitational Lensing Experiment (OGLE) survey over several transit epochs. Instead, we adopted their reported mid-time of transit and used that value in parts of the TTV analysis described in Section 4.

We fit all the other light curves for the transits central time, T_c, the planet-to-star radius ratio (R_p/R_s), the orbital inclination (i) and a quadratic limb darkening law, with u_1 and u_2 as the linear and quadratic limb darkening coefficients. We also fit a linear function of the flux versus time ($Y_{\rm int}$ and $Y_{\rm slope}$) in order to remove systematics in the light curves, which are mostly produced by changes in the airmass during the observations. The amount of correlated and uncorrelated noise is also estimated in each light curve using the wavelet-based method proposed by Carter & Winn (2009), where

Table 2. Results of the joint fit of the 19 transits of OGLE-TR-113b.

Simultaneous fitted parameters		
a/R_s	$6.44^{+0.04}_{-0.05}$	
(R_p/R_s)	$0.14436^{+0.00096}_{-0.00088}$	
i (deg)	$89.27^{+0.51}_{-0.68}$	
Limb darkening	u_1	u_2
R	$0.67^{+0.15}_{-0.18}$	$-0.03^{+0.29}_{-0.25}$
g', V	$0.733^{+0.094}_{-0.089}$	$0.14^{+0.14}_{-0.15}$
K	$0.20^{+0.25}_{-0.15}$	$0.09^{+0.29}_{-0.33}$
i', I	$0.299^{+0.061}_{-0.055}$	$0.43^{+0.10}_{-0.12}$

the noise parameters, σ_w (for the white noise) and σ_r (for the correlated noise), are fitted from the light curves assuming the correlated noise follows a power spectral density varying as $1/f$.

We fixed the values of the orbital eccentricity, e, and longitude of periastron, ω, to zero, and we adopted a fixed orbital period for the system of $P = 1.432\,474\,25$ d from A10.

Having several transit epochs is advantageous to refine the values of some of the system's parameters, such as i, R_p/R_s and a/R_p. Therefore, we fit for those parameters using all the light curves, simultaneously, while letting T_c vary individually for each transit. We found that we cannot produce reliable limb darkening fits on individual light curves. The fits also had problems distinguishing between very similar filters, e.g. between the Gemini i' and the MagIC i' filters, or the Gemini g' and V filters. We got around this problem by fitting both limb darkening coefficients (u_1 and u_2) simultaneously for all the *same* filter light curves, i.e. i', g', R and K, where we assumed that the limb darkening coefficients for similar filters were the same. Furthermore, based on Csizmadia et al. (2012), we do not fix the limb darkening coefficients to theoretical predictions but leave them as free parameters. The limb darkening coefficients obtained from the joint analysis of each filter are summarized in Table 2.

We ran 10 different MCMC chains of 10^5 links each, discarding the first 10 per cent to avoid any bias introduced by initial values of the fitted parameters. Our fits yield refined values for i, R_p/R_s and a/R_p, which are summarized in Table 2. In Table 3, we show the central time obtained for each transit. The raw transit light curves are shown in Fig. 1, together with their best model fits. All the data are available online in tables including the times and normalized fluxes of each transit; Table 4 shows an excerpt of those tables.

We note in the $E = 1471$ light curve a signature that can be attributed to star spot occultations of the planet during the transit. The transits $E = 192$, 793 and 992 also show *bumps* in the light curves during transit but with very low amplitudes. Moreover, A10 reported that the bump in the $E = 793$ light curve was produced by a rapid seeing variation. The large time span between these *detections* prevents us from carrying out a more detailed study of the rotational period of the star.

4 TRANSIT TIMING ANALYSIS

To ensure a uniform timing analysis for all transits, we converted the time stamp in each new light-curve frame to Barycentric Julian Days in the Barycentric Dynamical Time standard system (BJD_{TDB}), as suggested by Eastman, Siverd & Gaudi (2010), before modelling the light curves. For the literature light curves we used the times provided by A10, already converted to BJD_{TDB}.

Table 3. Central times of the transits of OGLE-TR-113b obtained from the light-curve fitting with TAP and its residuals from the timing analysis.

Epoch	Residuals (ppm)	$T_c - 2450000.$ (BJD_{TDB})	(O−C) lineal (s)	(O−C) quad (s)
−795	–	$2325.79897^{+0.00082}_{-0.00082}$	−38	−32
0	0.0013	$3464.61725^{+0.00027}_{-0.00026}$	15	16
5	0.0019	$3471.77859^{+0.00042}_{-0.00041}$	−75	−73
7	0.0027	$3474.64382^{+0.00058}_{-0.00057}$	−51	−49
192	0.0017	$3739.65294^{+0.00052}_{-0.00053}$	56	57
243	0.0087	$3812.70856^{+0.00060}_{-0.00061}$	4	5
465	0.0014	$4130.71840^{+0.00055}_{-0.00054}$	36	37
738	0.0013	$4521.78374^{+0.00023}_{-0.00023}$	6	6
779	0.0029	$4580.51525^{+0.00051}_{-0.00052}$	9	9
793	0.0010	$4600.56977^{+0.00014}_{-0.00014}$	−3	−3
946	0.0020	$4819.73961^{+0.00040}_{-0.00040}$	97	98
953	0.0014	$4829.76632^{+0.00030}_{-0.00032}$	44	44
969	0.0011	$4852.68574^{+0.00026}_{-0.00024}$	28	29
990	0.0018	$4882.76777^{+0.00023}_{-0.00023}$	33	33
992	0.0016	$4885.63248^{+0.00029}_{-0.00030}$	12	13
1006	0.0017	$4905.68710^{+0.00033}_{-0.00032}$	10	10
1045	0.0017	$4961.55291^{+0.00017}_{-0.00017}$	−53	−52
1471	0.0013	$5571.78736^{+0.00027}_{-0.00026}$	−46	−45
2530	0.0034	$7088.77895^{+0.00056}_{-0.00058}$	−3	4
2585	0.0025	$7167.56574^{+0.00058}_{-0.00058}$	54	62

Table 4. Raw light curves of the nine transits of OGLE-TR-113b presented in this work. We also included the best fitted model with TAP. Full table is available in the online journal.

Exp. Midtime (BJD_{TDB})	Normalized Raw flux	Modelled Flux	Residuals
$E = 192$			
2453739.605173	1.003039	1.001438	0.001601
2453739.606043	1.001873	1.001420	0.000453
2453739.609924	1.002305	1.001340	0.000965
–	–	–	–

We derived an Observed minus Calculated (O-C) diagram for the 19 modelled transits and the mid-time reported by Konacki et al. (2004) for the transit on $E = -795$, using the constant period ephemeris equation from A10, which has the form:

$$T_c = T_0[\mathrm{BJD}_{TDB}] + P * E, \quad (1)$$

where T_c is the predicted central time of transit in a given epoch E, T_0 is the reference time of transit and P the orbital period. The values of T_0 and P adopted in this case are $T_0 = 2453464.61762\mathrm{BJD}_{TDB}$ and $P = 1.432\,474\,25$ d.

It is clear that the central times of the 20 transits do not follow this ephemeris which can be due to accumulated uncertainty over time on the parameters of the fit. Therefore, in an attempt to correct for those accumulated uncertainties, we perform a new weighted linear fit to the transit mid-times. This correction yields the following new ephemeris equation:

$$T_c = 2453464.61708(14)[\mathrm{BJD}_{TDB}] + 1.43247506(14) * E, \quad (2)$$

where the parameters and their 1σ uncertainties are drawn from their posterior probability distribution obtained from a MCMC

Table 5. Results of the linear and quadratic fits of the transit times of OGLE-TR-113b.

Fit	Period (d)	T_0 (BJD$_{TDB}$)	δP ($\times 10^{-10}$ d)	$\dot{P}$ (msyr^{-1})	χ^2	$\chi^2_{\rm red}$	BIC	RMS (s)
Linear	1.432 475 06(14)	2453464.61708(14)	–	–	42	2.3	48	42
Quadratic	1.432 475 10(28)	2453464.61706(16)	-0.5 ± 2.5	-1.0 ± 6.0	42	2.5	51	41

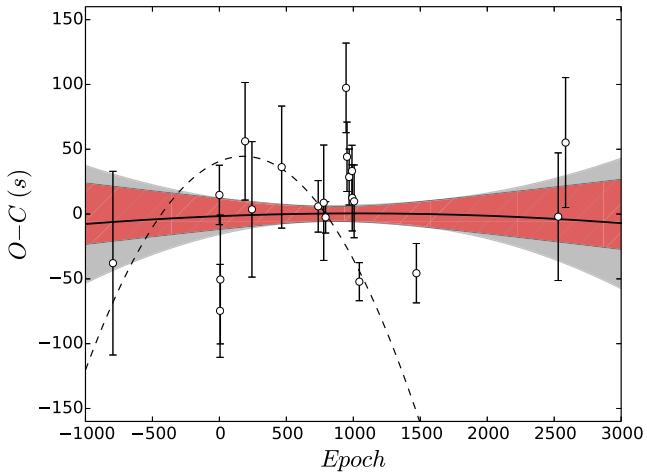

Figure 2. Updated (O−C) diagram for the transit mid-times of OGLE-TR-113b using a constant period ephemeris (equation 2). The $\pm 1\sigma$ errors of the linear ephemeris is represented by the red-hatched region. The RMS of the residuals is 42 s. The linearly changing period ephemeris (equation 3) is represented by the solid black line and its $\pm 1\sigma$ errors by the grey region. The dashed line represents the corrected changing period function reported by A10.

analysis performed with the EMCEE sampler implemented by Foreman-Mackey et al. (2013). After correcting the ephemeris for this new linear equation we obtain the timing residuals shown in the Fig. 2. The red-hatched region represents the $\pm 1\sigma$ limits of the linear function. This new linear fit has a reduced chi-squared of $\chi^2_{\rm red} = 2.3$ and a Bayesian Information Criterion (BIC) of 48, while the dispersion of the timing residuals is RMS = 42 s.

Using the central times of 11 transits, A10 noticed a hint of an orbital decay for OGLE-TR-113b of $\dot{P} = -60 \pm 15$ ms yr^{-1}. The corrected version of the changing period function (private communication) suggested by A10 is represented by the dashed-line in Fig. 2. To check if this variation is still detected in our extended data set we fit our central times for the 20 transit epochs for a linearly changing-period of the form (using the same notation from A10):

$$T_c = T_0[\mathrm{BJD}_{TDB}] + P * E + \delta P * E(E-1)/2, \quad (3)$$

where δP represents the variation of the orbital period per epoch ($P = P_0 + \delta P * E$). The quadratic fit is represented by solid curve in Fig. 2. Due to the low amplitude of the quadratic term of the fit, the timing residuals of this fit are very similar to the linear case. The $\pm 1\sigma$ error of the quadratic function is represented by the grey region of Fig. 2.

We obtain a $\delta P = (-0.5 \pm 2.5) \times 10^{-10}$ d, which is fully consistent with a constant orbital period ($\delta P = 0$) in contrast with the value reported by A10 of $\delta P = (-2.74 \pm 0.66) \times 10^{-9}$ d. The dispersion of the mid-times residuals of this quadratic fit is almost identical to the linear case ($RMS = 41$ s) and with marginal differences in the statistical indexes ($\chi^2_{\rm red} = 2.5$ and BIC = 51). In addition, when we examine the change in period per year, we obtain $\dot{P} = -1.0 \pm 6.0$ ms yr^{-1}, which is significantly smaller than the rate observed before. The results of the linear and quadratic fits are shown in Table 5.

As mentioned, the mid-time of Konacki et al. (2004) epoch is the result of a combination of several low cadence light curves and therefore is not well suited for timing analysis. Thus, we explore the influence of this mid-time in our ephemeris fits by repeating our analysis without this epoch. We observed no major differences in the results of the weighted fits by excluding the $E = -795$ transit, e.g. the quadratic term is consistent with zero ($\delta P = (0.2 \pm 2.8) \times 10^{-10}$ d).

Additionally, we find no evidence of periodic variations in the timing residuals of the linear fit. We also use the Anderson–Darling test (Anderson & Darling 1954) to probe if the residuals of the linear fit are drawn from a Normal distribution. According to this test, the residuals sample comes from a normal distribution with 85 per cent of confidence.

Finally, we investigate the robustness of our results by exploring the significance of the findings reported in A10 using our mid-times. We therefore, re-estimate equation (3) using only our values of T_c from the literature transits, i.e. the light curves in A10. We obtain a $\dot{P} = -44 \pm 21$ ms yr^{-1} which is smaller but fully consistent with the value obtained by A10. It is clear that by adding our new transits in the O−C diagram, extending the system monitoring time span from 6 to more than 13 yr, the quadratic term is much less significant than the one obtained with only the transits up to 2009 ($E \sim 1000$).

5 PERTURBER MASS LIMITS

Using the limits imposed by our TTV analysis (RMS = 42 s), we investigate the mass of additional perturbing bodies in the system, which could produce the observed dispersion in the transit mid-times. For this, we use the MERCURY integrator code (Chambers 1999) to generate a set of dynamical simulations of the OGLE-TR-113 system. We use circular and coplanar orbits and set the physical properties of the star and OGLE-TR-113b to the values listed in Table 2. The initial orbit of the perturber was calculated from Kepler's third law by using an orbital period in the range $P_{\rm per} = 0.1 - 4.5 P_{\rm tran}$ in steps of 0.05 or $0.005 P_{\rm tran}$ when more resolution was needed, e.g. near Mean Motion Resonances (MMRs). $P_{\rm tran}$ is the OGLE-TR-113b orbital period derived in this work. The perturber mass varied from 0.1 to 1500 $M_\oplus$; this variation depends on the calculated TTV (see below). We let the system evolve for 15 yr but we save transit times only after the first 3 yr to avoid any perturbation induced by initial conditions. For each simulation we imposed the condition that the calculated period of the *transiting planet* did not deviate more than 60 s from the real period of OGLE-TR-113b. If the deviation was larger, then the initial conditions of the transiting planet's orbit for that specific simulation were changed in order to obtain the desired orbital period. Usually small changes in the initial location of the planet were necessary. Then, for each simulation the RMS of the TTVs was calculated, increasing the perturber mass until an RMS = 45 s was reached. Close to this mass level, we ran again the simulations using a mass step of 0.1 or 1.0 $M_\oplus$, depending on the required precision. The results of these

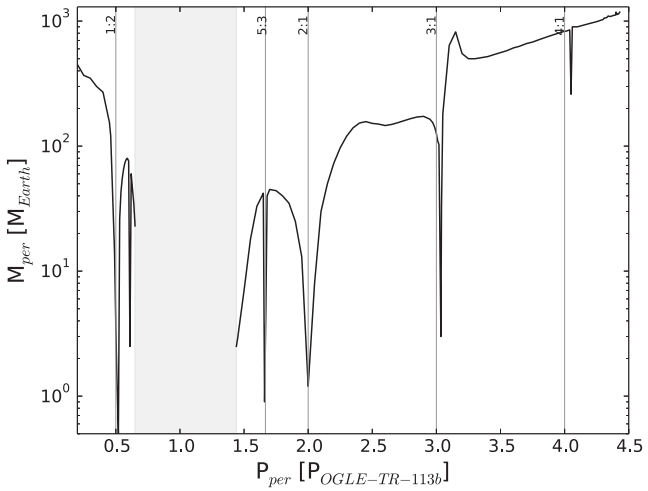

Figure 3. Mass as a function of its orbital period of a hypothetical perturber in the OGLE-TR-113 system. The grey strip and vertical lines represent the instability region of the system and the location of the principal MMRs, respectively.

dynamical simulations are shown in Fig. 3. By using the limits of our timing analysis, we discard perturbers with masses larger than 0.5 and 0.9 $M_\oplus$ near the 1:2 and 5:3 MMRs, 1.2 $M_\oplus$ near the 2:1 MMR and 3.0 $M_\oplus$ near the 3:1 MMR. While we agree with the mass limits placed by A10 in the 1:2 and 2:1 MMRs, our 5:3 and 3:1 MMR limits are almost one order of magnitude more strict.

6 CONCLUSIONS

We have observed nine new transits of OGLE-TR-113b as part of TraMoS project extending the time span of the observations from 6 yr to over 13 yr. By performing a simultaneous timing analysis of these transits and literature transits we tested the tentative detection of orbital period decay for this planet reported by A10.

Our timing analysis of 20 transit epochs discards the presence of a linearly changing period of OGLE-TR-113b. We obtain a $\delta P = (-0.5 \pm 2.5) \times 10^{-10}$ d which is fully consistent with a constant orbital period for OGLE-TR-113b. Our updated $\dot{P} = -1.0 \pm 6.0$ ms yr^{-1} is about one order of magnitude smaller than the value reported by A10 and consistent with zero.

For a large sample of Kepler planet hosts, Penev et al. (2012) set a strong limit on the tidal quality factor of $Q_\star \geq 10^7$. In the case of OGLE-TR-113b, using a 1σ value based on our measured orbital decay, i.e. $\dot{P} = -7.0$ ms yr^{-1}, stellar and planetary masses from Southworth (2012), and equations 5 and 7 from Birkby et al. (2014) we obtain $Q_\star \sim 2.6 \times 10^4$ for this system. Those values of $Q_\star$ imply a $T_{\rm shift} = 157$ s after 13.2 yr, which is clearly not observed in the O−C diagram in Fig. 2. Using $\dot{P} = -1.0$ ms yr^{-1}, we obtain $Q_\star \sim 1.8 \times 10^5$ and a $T_{\rm shift}$ of 22 s, which is fully consistent with the RMS of the timing residuals. Therefore, based on our timing analysis we can discard $Q_\star < 10^5$. A time shift of 100 s is expected in 7 more years (i.e. in a total of 20 yr of monitoring) if $Q_\star \sim 10^5$ and $\dot{P}$ is of only a few ms yr^{-1}. Only a 10 s shift is expected if $Q_\star \sim 10^6$ instead. Additionally, based also on the timing analysis of the transits, we can place strict constraints on the mass of additional bodies in the system. We discard planets with masses larger than 0.5, 0.9, 1.2 and 3.0 $M_\oplus$ near the 1:2, 5:3, 2:1 and 3:1 MMRs. Finally, with the homogeneous analysis of these data and the literature transits, we update the physical properties of this system.

ACKNOWLEDGEMENTS

Based on observations obtained at the Gemini Observatory, which is operated by the Association of Universities for Research in Astronomy, Inc., under a cooperative agreement with the NSF on behalf of the Gemini partnership: the National Science Foundation (United States), the National Research Council (Canada), CONICYT (Chile), the Australian Research Council (Australia), Ministério da Ciência, Tecnologia e Inovação (Brazil) and Ministerio de Ciencia, Tecnología e Innovación Productiva (Argentina).

Based on observations obtained at the Southern Astrophysical Research telescope, which is a joint project of the Ministério da Ciência, Tecnologia, e Inovação (MCTI) da República Federativa do Brasil, the US National Optical Astronomy Observatory (NOAO), the University of North Carolina at Chapel Hill (UNC), and Michigan State University (MSU).

SH acknowledges financial support from the Spanish Ministry of Economy and Competitiveness (MINECO) under the 2011 *Severo Ochoa* Program SEV-2011-0187. PR acknowledges Fondecyt #1120299, Anillo ACT1120. DM is supported by the Millennium Institute of Astropysics MAS from the Ministry of Economy ICM grant P07-021-F. PR and DM are also supported by the BASAL CATA Center for Astrophysics and Associated Technologies PFB-06.

REFERENCES

Adams E. R., López-Morales M., Elliot J. L., Seager S., Osip D. J., 2010, ApJ, 721, 1829 (A10)
Agol E., Steffen J., Sari R., Clarkson W., 2005, MNRAS, 359, 567
Anderson T. W., Darling D. A., 1954, J. Acoust. Soc. Am., 49, 765
Birkby J. L. et al., 2014, MNRAS, 440, 1470
Bouchy F., Pont F., Santos N. C., Melo C., Mayor M., Queloz D., Udry S., 2004, A&A, 421, L13
Carone L., Pätzold M., 2007, P&SS, 55, 643
Carter J. A., Winn J. N., 2009, ApJ, 704, 51
Chambers J. E., 1999, MNRAS, 304, 793
Csizmadia S., Pasternacki T., Dreyer C., Cabrera J., Erikson A., Rauer H., 2012, A&A, 549, A9
Diaz R. F. et al., 2007, ApJ, 660, 850
Eastman J., Siverd R., Gaudi B. S., 2010, PASP, 122, 935
Foreman-Mackey D., Hogg D. W., Lang D., Goodman J., 2013, PASP, 125, 306
Gazak J. Z., Johnson J. A., Tonry J., Dragomir D., Eastman J., Mann A. W., Agol E., 2012, Adv. Astron., 2012, 30
Gillon M., Pont F., Moutou C., Bouchy F., Courbin F., Sohy S., Magain P., 2006, A&A, 459, 249
Holman M. J., Murray N. W., 2005, Science, 307, 1288
Hoyer S., Rojo P., López-Morales M., Díaz R. F., Chambers J., Minniti D., 2011, ApJ, 733, 53
Hoyer S., Rojo P., López-Morales M., 2012, ApJ, 748, 22
Hoyer S. et al., 2013, MNRAS, 434, 46
Konacki M. et al., 2004, ApJ, 609, L37
Levrard B., Winisdoerffer C., Chabrier G., 2009, ApJ, 692, L9
Matsumura S., Peale S. J., Rasio F. A., 2010, ApJ, 725, 1995
Miralda-Escudé J., 2002, ApJ, 564, 1019
Pätzold M., Carone L., Rauer H., 2004, A&A, 427, 1075
Penev K., Sasselov D., 2011, ApJ, 731, 67
Penev K., Jackson B., Spada F., Thom N., 2012, ApJ, 751, 96
Pietrukowicz P. et al., 2010, A&A, 509, A4
Sasselov D. D., 2003, ApJ, 596, 1327
Snellen I. A. G., Covino E., 2007, MNRAS, 375, 307
Southworth J., 2012, MNRAS, 426, 1291
Udalski A., Szewczyk O., Zebrun K., Pietrzynski G., Szymanski M., Kubiak M., Soszynski I., Wyrzykowski L., 2002, Acta Astron., 52, 317

SUPPORTING INFORMATION

Additional Supporting Information may be found in the online version of this article:

Table 4. Raw light curves of the nine transits of OGLE-TR-113b presented in this work. (http://mnras.oxfordjournals.org/lookup/suppl/doi:10.1093/mnras/stv2362/-/DC1).

Please note: Oxford University Press is not responsible for the content or functionality of any supporting materials supplied by the authors. Any queries (other than missing material) should be directed to the corresponding author for the article.

This paper has been typeset from a TEX/LATEX file prepared by the author.